Effects of Injection Pressure on Spray Atomization Characteristics with Measurement Technique Cross-Validation

J. D. Lee[1], A. Saha[1], S. Basu[2], R Kumar[1]
[1]University of Central Florida, Orlando, USA
[2]Indian Institute of Science, Bangalore, USA
jd2lee86@gmail.com, abhishek.saha@ucf.edu, sbasu@mecheng.iisc.ernet.in and ranganathan.kumar@ucf.edu

Abstract

This paper deals with an experimental study of the breakup characteristics of water emanating from pressure-swirl hydraulic injector nozzles. The experiments were conducted using two nozzles with different orifice diameters 0.3mm and 0.5mm and injection pressures (0.3-4MPa) which corresponds to Re_p = 7,000-26000. The effects of Reynolds number on the spray angle and other atomization characteristics were studied. Three laser diagnostic techniques were utilized: Shadowgraph, PIV (Particle Image Velocimetry), and PDPA (Phase Doppler Particle Anemometry) for a complete study of the atomization process. The comparison among the three techniques compared well with each other. Limitations of these techniques in different flow regimes related to the breakup are provided. Results indicate that velocity exhibits a logarithmic decay axially. The diameter decreases away from the nozzle, however, at some distance, the droplets begin to coalesce to make the effective diameter larger. These effects are seen to be functions of Reynolds number.

Introduction

Atomization of liquid film or ligament from an injector nozzle is critical for various industry applications, such as power generation, food or pharmaceutical powder formation, and thermal sprays. Most of the aero-engines and IC engines use liquid fuel and atomization techniques to obtain a homogenous mixture at different equivalence ratios. However, depending on the design of the pre-vaporizers and combustors, different nozzles are used in engines. This mixture quality, not only determines the combustion performance and efficiency of the power generation unit, but also controls the emission. Each application utilizes different atomizers and liquids, and results in a wide range of spray dynamics and mixture quality. Thus, for each type of atomization technique, the fundamentals of spray dynamics, such as spray formation, liquid breakup length, and droplet breakup regimes needs to be understood. It is critical to understand and adequately predict these characteristics based on the operating conditions (such as atomizing pressure, flow rate) and physical properties of the atomizers (such as cone angle, nozzle geometry).

In modern engines, the liquid fuel is injected into the combustion zone either by an air-blast or hydraulic nozzle. The hydrodynamic instabilities of liquid sheets leading to breakup are predominant in air-blast atomizers [1-3]. The hydraulic nozzle produces liquid atomization by forcing the liquid through a single narrow annulus under a pressure gradient [4]. On the other hand an air-blast nozzle has two orifices that use an air-liquid momentum ratio to induce atomization [3]. For most of the hydraulic nozzles, atomization is induced by pressure which causes the liquid to breakup/atomize.

The breakup process consists of two steps: a) A primary breakup regime induced by hydrodynamic instabilities and relatively large drag forces that cause the formation of ligaments or other irregular liquid elements and b) a secondary breakup regime which is caused by aerodynamic instabilities resulting in larger droplets deforming and breaking up into smaller droplets [4-6]. The secondary breakup process will continue until the droplets approach their critical Weber number. At this point, the breakup process terminates and the process of droplet coalescence is initiated. In order to understand the breakup process for hydraulic nozzles and to establish models for droplet distributions for liquid jet nozzles, researchers have used various optical techniques such as PDPA and LDV to investigate the effects of various system parameters, i.e. viscosity, density, and surface tension on the initial distribution of droplet diameters and velocities [2, 7-9]. It has been reported that system parameters, such as viscosity, density and nozzle diameter affects the spreading (cone) angle and breakup [10]. Senecal et. al [11] reported two distinct regimes of film atomization for cylindrical jet hydraulic nozzles; long and short wave induced film breakup similar to the findings by Sivakumar and Kulkarni [3] who reported five regimes for air-blast nozzles. Senecal et al. [11] also found that different types of film breakups are dependent on Weber number. Using high speed imaging, Wahono and Honnery [12] qualitatively visualized the spray structure to understand the types of instabilities and ligament formations that are exhibited in hydraulic jet nozzles. Even with these experimentations reported by researchers, there was no significant model available that correlated the effects of injection pressure, on droplet profiles and breakup regimes, in a pressure-swirl induced hydraulic nozzles.

The main objectives of this research are to experimentally investigate the effects of injection pressures on the liquid breakup regimes including droplet coalescence in a series of hollow cone hydraulic atomizing nozzles. This was done using various optical techniques such as Shadowgraph, PIV, and PDPA. This study will also identify the different spray regimes encountered and how they are affected by the different hydraulic nozzles and injection pressures.

Experimental Setup

The schematic diagram of the experimental setup utilized in this study is shown in Figure 1. The system consists of an autoclave (injection pressures up to 7.5MPa), test nozzles, and a three axis transverse system which precisely controlled the placement of the nozzle (25.4 µm increments). Both the Shadowgraph and PIV utilized a 532nm (maximum energy 70 mJ per pulse) dual pulsed Nd-Yag laser (4 mm beam diameter) with an interline CCD camera (pixel resolution of 1376 x 1040) synchronized to the laser pulse. To perform the Shadowgraph, a 90^o turning mirror and a circular diffuser (20°) were used to convert the 4 mm beam into a diffused mode to provide adequate backlighting for the spray. The CCD camera along with a Navitar zoom lens was placed in front of the spray, parallel to the light source (Figure 1a). The setup with the zoom lens allowed a viewing window of 0.9 mm x 0.9 mm with a depth of field around 200 µm. Using the similar setup, PIV was achieved by replacing the diffuser with an appropriate plano-concave lens which converted the circular beam into a ~500µm thick laser sheet with a height of around 15 mm. The laser was positioned such that the vertical light sheet passed through the center of the spray. The CCD camera was repositioned from parallel to perpendicular viewing of the light source (Figure 1b). The pulse duration of the laser was on the order of 10 ns. The setup was operated at 5 fps. The time lag between two pulses (Δt) was varied to determine its effect on the velocity field. After a few iterations it was determined that for Shadowgraph and PIV 2 µsec is optimum for the flow field near the nozzle exit and around 5 µsec further downstream of the spray. The PDPA system consisted of a 632 nm He-Ne laser with adjoining photo-multiplier tube receiver set at the appropriate receiving angle of 70° based on the refraction angle of water (Figure 1c).

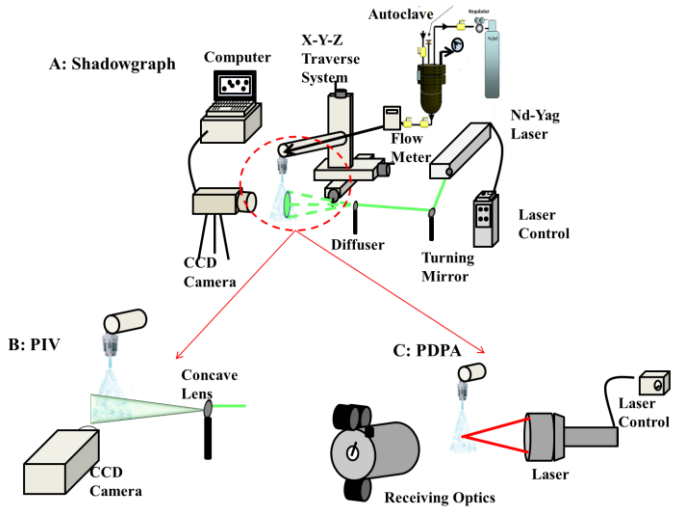

Figure 1: Schematic of the Techniques Utilized - A: Shadowgraph, B: PIV, C: PDPA

The data reported in this paper was taken on a vertical plane which passed through the center of the nozzle. For PIV and shadowgraph, the calibration and proper focusing of the CCD camera was done using grid paper which was placed under the nozzle attached vertically to the traverse system. For the PDPA the two laser beams were allowed to intersect directly below and in the center of the nozzle exit by moving the nozzle with the traverse system to measure diameter and velocity. In order to capture data below the nozzle tip, the nozzle was moved using the traverse system, without disturbing the optical setup. The autoclave was pressurized with both water and air ranging from 0.3-4 MPa and was allowed to equilibrate for 10 minutes. The water is then injected into atmospheric conditions (25°C and 1.01kPa) through two different hydraulic nozzles. The droplet diameter and velocity were measured at several axial locations throughout the spray. The diameter and velocity were calculated by Shadowgraph utilizing an in-house algorithm with edge detection methods from Matlab. A background subtraction was needed to eliminate background noise that arose from the non-uniformity of the diffuser. A series of images (200 image pairs) was used to generate a histogram for the droplet diameter and compared to PDPA measurements, which consisted of 10000 samples, at the same location for a cross validation comparison. A set of 200 image-pairs was averaged to calculate the velocity vectors. This number was determined to be sufficient to minimize the uncertainty from grid generation, correlation and peak validation.

Shadowgraph was used not only for visual inspection of the different breakup regimes and the nozzles spray characteristics, but also to measure the velocity and droplet diameter. The PIV technique was utilized for velocity measurements. PDPA is traditionally a point measurement technique while PIV and Shadowgraph are field measurements

and not usually comparable. Since the PDPA laser beams are of the order of 1 mm in diameter, the area in which the measurements are made is of the same order as the other two methods, thus allowing direct comparison. Another objective of using different techniques was also to compare among the different techniques to ensure accurate results at different zones of the spray.

Results and Discussion

The study used two hydraulic nozzles supplied by Parker Hannifin. The nozzles are classified as Flow Number (FN) 0.4 and 1.7. The Flow Number is characterized as the ratio of the mass flow rate (lbm/hour) and the square root of the differential pressure (psi). Results were plotted vs. Reynolds number. Reynolds number can be determined using a velocity scale based on the pressure drop [12], $U_{scale} = \sqrt{\frac{2.\Delta P}{\rho}}$; $\mathrm{Re}_p = \frac{\rho.D}{\mu}\sqrt{\frac{2.\Delta P}{\rho}}$, where D is nozzle diameter, μ is liquid viscosity, ρ is liquid density and ΔP is differential pressure. A non-dimensional mass flow rate, $\dot{m}^* = \frac{\dot{m}_{actual}}{\dot{m}_{scale}}$ may be defined where $\dot{m}_{scale} = U_{scale}.A.\rho$ and $\dot{m}_{actual} = (FN).\sqrt{\Delta P}$. Using the definition of U_{scale}, $\dot{m}^* = \frac{(FN)}{A.\sqrt{\rho}}$. The two nozzles with FN of 0.4 and 1.7 correspond to $\dot{m}^*$ = 0.2 and $\dot{m}^*$ = 0.29.

The three main parameters that influence the spray dynamics are the spray cone angle, film length, and the maximum wave amplitude, which will be described next.

Cone Angle and Film Length:

The cone angle measurement was performed using Shadowgraph. The captured images were processed using Matlab edge detection procedure to determine the edge of the flow as indicated by the diagonal red lines in Figures 2a and 2b. A series of 20 images for each pressure was used as a statistical average. As shown in Figure 2c for $\dot{m}^*$ = 0.2 (0.3 mm diameter) nozzle, the spray angle monotonically increases from 30° (at Re_p = 10,500) before attaining a constant value of 78° around Re_p = 21,000. On the other hand, for $\dot{m}^*$ = 0.29 (0.5mm diameter) nozzle, the same trend was seen except that the spray angle varied from 75° to 100° (Figure 2c).

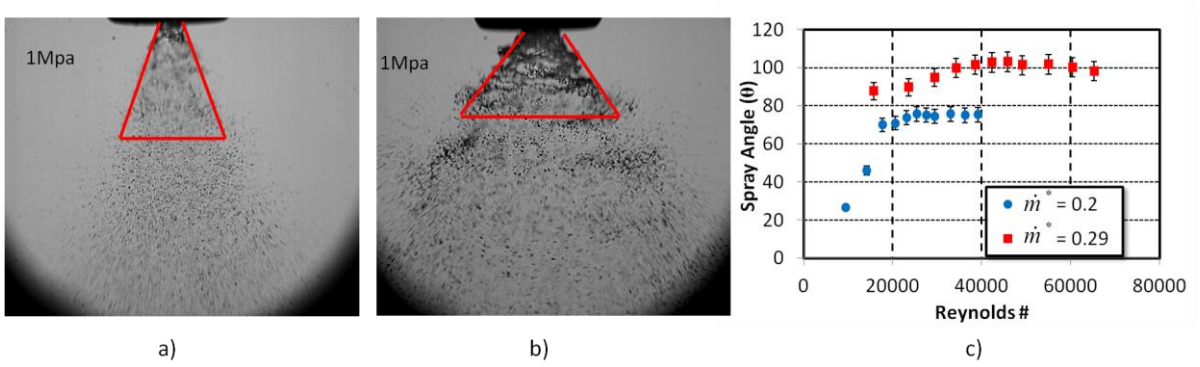

Figure 2: Pressure effects on spray cone angle – a) High speed image of $\dot{m}^*$ = 0.2, b) High speed image of $\dot{m}^*$ = 0.29, c) Plot of the effects of Reynolds number on the spray cone angle.

To determine the film length and the maximum wave amplitude, each image frame was inspected and the pixel lengths were measured. An average from 20 images is reported here. Figure 3 shows the film length and the maximum wave amplitude where the film length is indicated by the red line. Maximum wave amplitude denotes the radial distance from the centerline of the spray to the peak of the wave just before the breakup of the liquid film. The film length is the vertical distance from the nozzle tip where liquid sheet begins to disintegrate into ligaments. These two parameters are found to be correlated. Figure 3c and 3d show both the maximum wave amplitude and film length as a function of injection pressure. One can notice in Figure 3c that the trends for the maximum wave amplitude are opposite for two nozzles. These opposite trends show that the instabilities that cause breakup in the nozzles are of different types. At low pressure, the instabilities in the liquid film for the small nozzle ($\dot{m}^*$ = 0.2) converge into a sharp point with small amplitudes and long wavelengths that induce breakup. With increase in pressure, the flow angle sharply increases resulting in outward flow expansion and the instabilities become shorter in wavelengths and larger in amplitude. Thus,

the wave amplitude reduces with increase in pressure until it attains a constant value at around 1.2 MPa. On the other hand, the flow for the larger nozzle expands outwards with short wavelengths and larger amplitudes. The cone angle does not increase significantly with the pressure for this nozzle. The larger nozzle ($\dot{m}^*$ = 0.29) experiences this type of instability breakup for the majority of cases. It can also be noted that at a certain pressure for both nozzles, the maximum wave amplitude becomes constant which directly corresponds to when the spray angle becomes constant due to the aforementioned reason. When the maximum wave amplitude is non-dimensionalized with the nozzle diameter the same trends are seen at low injection pressures but once the wave amplitudes become constant they merge into one location. This difference at low injection pressures is due to the two types of wavelengths experienced for the different nozzles. From Figure 3d, one can see that both nozzles follow the same trend for change in liquid length with pressure. The film length for the smaller nozzle is smaller than the larger nozzle which directly corresponds to the lower $\dot{m}^*$, which represents lower liquid momentum. This trend correlates well with the literature [4]. The film lengths reach an asymptotic value around 2MPa which directly correlates to when the spray angle becomes constant. This indicates that the film length is also directly dependent of the spray cone angle. With the same scaling approach that was done for the maximum wave amplitude the opposite is seen. At the low injection pressures both nozzles produce similar results but once the dimensional film length becomes constant a difference is seen between the two nozzles on the non-dimensional scale where $\dot{m}^*$ = 0.29 is larger. This is due to the difference in the mass flux which is much higher for the larger nozzle.

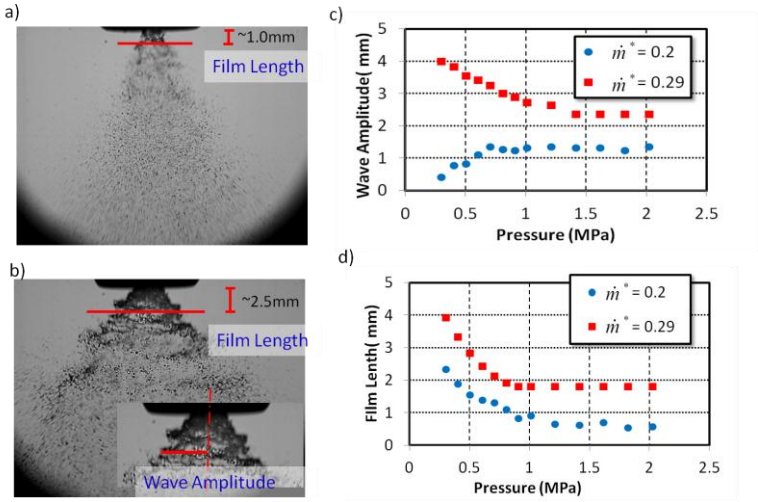

Figure 3: Pressure effects on wave amplitude and film length – a) High speed image of $\dot{m}^*$ = 0.2, b) High speed image of $\dot{m}^*$ = 0.29 (in inset location of wave amplitude is shown), c) Plot of the effects of pressure on the maximum wave amplitude, d) Plot of the effects of pressure on the film length.

Spray Profile:

In this section we will look into the spray profile along the centerline of the spray in the axial direction. Even though a hollow cone nozzle is utilized, data rate in the core was significant due to the swirling force associated with these nozzles. Although in the next section we will establish that validity of three different optical techniques, for the sake of simplicity the following analysis and figures reported in this section use data from PDPA. The variation of arithmetic mean diameter (AMD) along the centerline for different Reynolds numbers and different nozzles is reported in Figure 4a and 4b respectively. At any Reynolds number we tested and for any nozzle, the droplet diameter is seen to decrease initially and then increase along the centerline as we move away from the nozzle tip. This kind of nature of droplet diameter is also reported previously by other researchers [4]. However, we report measurements further downstream of the nozzle compared to the previously reported measurements. The trend suggests the presence of three droplet breakup/formation regimes, a) ligament formation (primary breakup), b) droplet deformation (secondary breakup), and c) droplet coalescence. This is also illustrated in Figure 5 where shadowgraph images are taken to show the breakup regimes. The liquid discharges out of the spray nozzle in the form of films, which break up due to aerodynamic instability in form of ligaments. This regime (Zone A in Figure 5), is primarily characterized by formation of ligaments and larger droplets through primary breakup. In the next zone, secondary breakup regime, the larger droplets formed in the previous zone goes through secondary atomization generating smaller droplets. Thus, the droplet diameter in this zone decreases rapidly as we move away from the nozzle. In the regime of droplet coalescence, smaller droplets collide and lose their momentum due to drag and form larger droplets. At the inception of this zone, the droplet diameter starts increasing with the distance from the nozzle. Due to coalescence, the droplets become larger and slower, which in-

creases probability of subsequent droplet-droplet collision resulting in coalescence. The transition between secondary atomization and droplet coalescence regimes can be identified by the inflection point in droplet diameter plot.

These transition points are observed to shift slightly towards the nozzle as Reynolds number increases (Fig 4a). With an increase in Reynolds number, the spray angle and the mass flow rate increases. The droplets with larger momentum show higher probability of coalescence, resulting in shorter primary and secondary breakup regimes. At very high Reynolds numbers (> Re_p = 25000) one can observe deviation from this droplet diameter trend. At such high Reynolds number, the spray induces a strong recirculation zone close to the nozzle exit. This results in a bimodal distribution of droplet diameter. One can observe strong presence of smaller diameter droplets besides regular sized larger droplets. Thus, the mean droplet diameter becomes smaller near the nozzle. However, beyond a certain distance from the nozzle tip, the recirculation becomes weak and smaller droplets disappear resulting in a diameter trend observed at lower Reynolds number. It was also observed that the recirculation zone, where droplet diameter is characterized by bimodal distribution, becomes shorter as the Reynolds number is increased past Re_p = 25000. In general, the droplet diameter trend becomes self-similar when the cone angle stops changing with increase pressure. However, the length of the recirculation zone near the nozzle exit alters with pressure even beyond this point.

With an increase in nozzle diameter (higher $\dot{m}^*$), one can see that the transition zones moves further away from the nozzle tip (Fig 4b). The nozzle with the larger orifice diameter ($\dot{m}^*$ = 0.29) generates a higher mass flow rate and denser spray, which allows for longer instability zones. Thus, the breakup regimes move away from the nozzle.

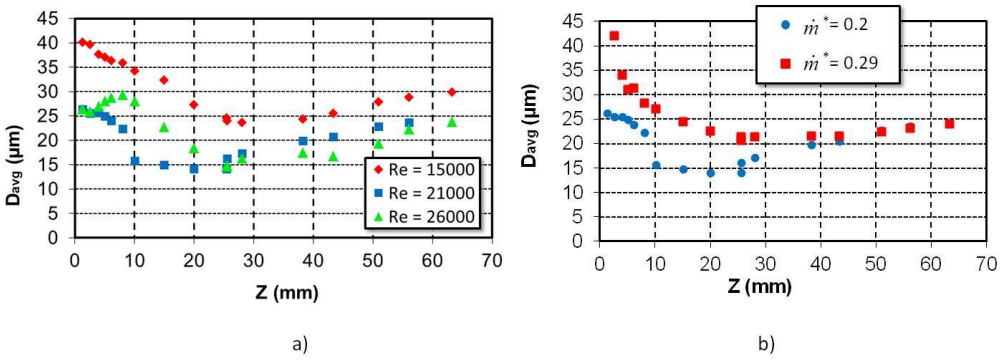

Figure 4: Diameter measurements along the centerline using PDPA – a) Pressure effects for $\dot{m}^*$ = 0.2, b) Nozzle effects at Re_p = 21,000

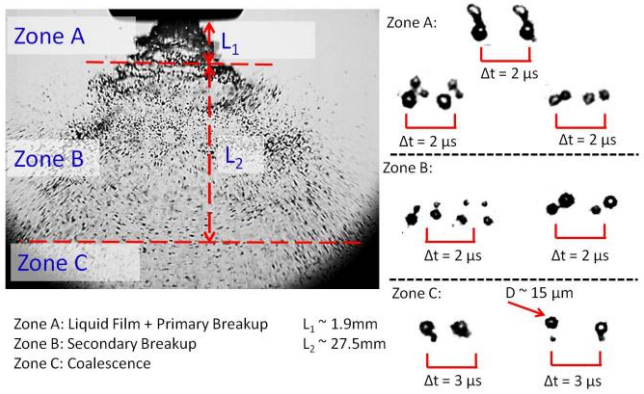

Figure 5: High speed images of breakup regimes.

Figure 6 shows the effects of Reynolds number and $\dot{m}^*$ on droplet velocity along the centerline. The results show that the droplet velocity decreases rapidly within the first 25.4 mm from the tip of the nozzle and then decreases at a slower rate until it reaches a constant value towards the end. This can be observed for both nozzles and all Reynolds number. It is important to note that as the Reynolds number increases the slope of the velocity within the first 25.4 mm becomes steeper due to the higher momentum flux for the higher Reynolds number and larger $\dot{m}^*$. Once the droplets reach a critical point of around 30mm for the current setup, the velocity becomes similar for all Reynolds numbers and

$\dot{m}^*$. One can argue that due to drag, the droplet lose most of its initial momentum by this length and attains a terminal velocity.

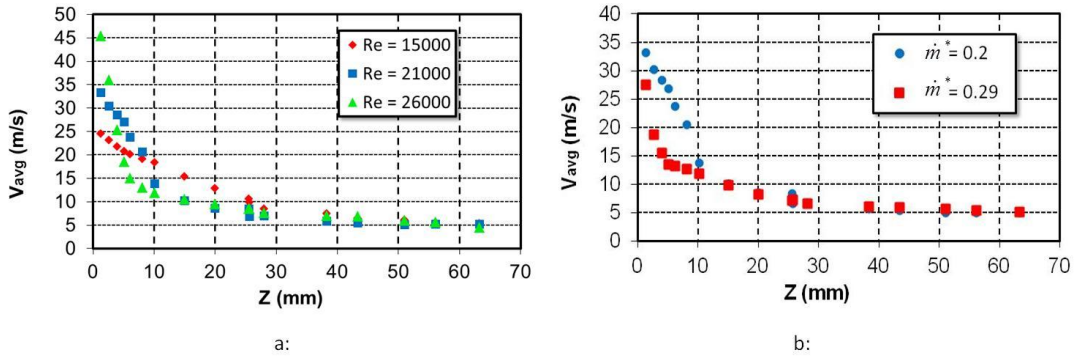

Figure 6: Velocity measurements along the centerline - A: Pressure effects for $\dot{m}^*$ = 0.2, B: Nozzle effects at Re_p = 21,000

Comparison of different optical techniques:

In order to validate and compare the measurements obtained by the three different techniques (Shadowgraph, PIV, PDPA), we measured the droplet diameter and velocity at different locations along the centerline (Figure 7a) for the smaller nozzle ($\dot{m}^*$ = 0.2) with orifice diameter of 0.3 mm at a single Reynolds number (Re_p = 15,000). Figure 7 shows velocity and diameter measured using these three techniques at different locations along the centerline. Although the results obtained from different techniques compared well for the velocity and diameter measurements, it should be mentioned that not all methods are possible to use at all the locations.

PIV:

In the primary breakup and at the beginning stages of secondary breakup regimes, the droplet sizes are rather large. High population of large droplets resulted in extremely dense spray, which increased noise in the Mie Scattering (used for PIV) significantly. Thus, PIV in this region was found to be impossible. It was later found that to obtain proper peak correlation between the two image pairs with acceptable uncertainties, measurements needed to be made further downstream where secondary breakup and droplet coalescence began to occur. At Re_p = 15,000, this occurred around 25.4 mm away from the nozzle where the droplet diameter was nearly half of the liquid film breakup regime. Although PIV measurements were possible as close as 12.7 mm from the nozzle, the uncertainty was quite high with no strong correlation peaks. Figure 7b shows that PIV velocity values indicate agreement with the other instruments at 25.4 mm, but not so closely at 12.7 mm. It can also be observed that as the distance increases beyond 25.4 mm the consistency between the three increases, indicating that confident data for PIV measurements can be obtained near the zone of transition from secondary breakup and coalescence. It was also noted that the secondary breakup zone is a function of Reynolds number which caused the accurate PIV measurements to shift. Although the secondary breakup regime moved towards the nozzle tip (occurred earlier) with an increase in Reynolds number, the zone of accurate PIV measurements was shifted downward axially to 35mm from the nozzle where the coalescence regime began. This shift happened due to the high liquid flow rate which increased the density of droplets further downstream. In addition, the droplet diameter reduces with an increase in Reynolds' number. At a low Reynolds number the cone angle is smaller resulting in a denser flow close to the nozzle, which further reduces the possibility of PIV measurements close the nozzle. For medium Reynolds numbers, (Re_p = 15,000-21,000) the spray angle is moderate allowing the droplets to expand further outward reducing droplet density of the spray allowing accurate PIV measurements to be possible. At Reynolds numbers greater than 24,000 the spray cone angle for this particular nozzle becomes constant, thus eliminating its effects on the PIV measurements. However, at these high Reynolds numbers, due to recirculation near the nozzle the chances of obtaining PIV measurements significantly reduces, thus shifting the zone of valid PIV measurements further downstream.

PDPA:

As a single point measurement, PDPA rendered successful data at locations closer to the nozzle where PIV data was not possible. However, PDPA had similar difficulties in delivering results for velocity and diameter measurements within 10 mm from the nozzle for majority of the Reynolds number. For low to moderate Reynolds numbers (Re_p = 10,500-25,000), the velocity and diameter measurements were reliable with instrument validation ranging from 20-65% spherical validation and 75- 95% depending on axial location and Reynolds number. Measurements were made close to the nozzle exit, where liquid films, ligaments, and non-spherical droplets are dominant. This corresponds to the beginning stages of secondary breakup. This region which varied as a function of Reynolds number caused the spheri-

cal validation percentage to be low, thus a longer sample time was needed to achieve 10,000 validated samples. As the Reynolds number increases, the film length becomes smaller enabling PDPA measurements at a higher validation level closer to the nozzle. At Re_p =15,000 PDPA measurements were possible at a distance of ~1.3-10 mm from the nozzle, with a satisfactory (70-75%) signal to noise validation percentage and (20-25%) spherical validation percentage. However, the presence of stretching droplets and ligaments increases the average diameter measured by the PDPA system causing the diameter measurements to be much larger than Shadowgraph. Droplets in the aspect ratio range of 0.9 to 1.1 were accepted as part of spherical validation. Since PDPA makes measurements in the vertical direction the diameter measurements are highly dependent on the aspect ratio. In the case of Shadowgraph discussed in the next section, droplet diameter measurements are not dependent on the aspect ratio. It was also observed that outside the ligament and primary breakup regime, the validation percentage increased (90-95% signal to noise validation and 60-65% spherical validation) due to the presence of spherical droplets generated by secondary breakup. Further downstream, at the other extreme of the spray, validation rate again decreased due to coalescence. This is evident in Figure 7c where the difference between the Shadowgraph and PDPA is the largest. As observed for PIV measurements, with increase in Reynolds number, the zone where PDPA measurement can be made with high confidence level shifted closer to the nozzle due to shorter film length. However, at Re_p = 26,000 the velocity and diameter started to show bimodal distribution at the points closer to the nozzle, which indicated the presence of strong recirculation. This is shown in Figure 6 when the diameter measurements increases near the nozzle at Re_p = 26000.

Shadowgraph:

Unlike PIV and PDPA which utilizes scattering or detecting frequency shifts through Doppler burst for measurements, the Shadowgraph technique depends on a pure observational approach for measurements. Thus, the Shadowgraph technique has less limitations arising from complex spray dynamics behaviors which restricted the use of PIV and PDPA in a concentrated zone. The only limitation present for Shadowgraph was due to the effects of film length and the ability to accurately capture the droplets shape (Fig 5). Owing to a high spatial resolution and small depth of field achieved through a zoom lens, both velocity and diameter measurements were possible throughout the centerline for all Reynolds numbers studied. The lens with high optical zoom and small depth of field allowed distinguishing between the droplets in the zone of interest facilitating better control for the user to utilize edge detection methods within Matlab. By selecting an optimum threshold gradient for the edge detection method, the uncertainty for the diameter measurements and velocity could be restricted to 2µm and 0.5m/s respectively. It was observed that near the nozzle exit, Shadowgraph over predicts the velocity and under predicts the diameter compared to other measurement techniques. The difference in the velocity points near the nozzle can be attributed to the presence of droplets with an aspect ratio less than unity in the beginning stages of secondary breakup regime. These droplets which are more elliptical in the vertical direction will have a longer duration within the PDPA measurement volume thus causing the velocity to be lower than droplets with aspect ratios greater than unity. On the other hand, Shadowgraph only looks at the center of each droplet and tracks this location from two consecutive images. This may have reduced the average velocity measured by PDPA. At the other extreme of the spray, despite good conformity of velocity measurements by different techniques, Shadowgraph over predicts the diameter compared to PDPA. It is significant to note that the PDPA measurements included 10,000 samples, while shadowgraph results were averaged over ~2,000 samples. Thus, far from the nozzle tip where coalescence starts to take place, the droplet density is less, and the Shadowgraph needs a larger sample for a better average. As a result, Shadowgraph tends to report higher average diameter. Although there is a small deviation from the values measured by different techniques as explained, they all show a very similar trend in the axial direction. This indicates that the Shadowgraph is a measurement technique which can be used at any spray regime with acceptable uncertainties.

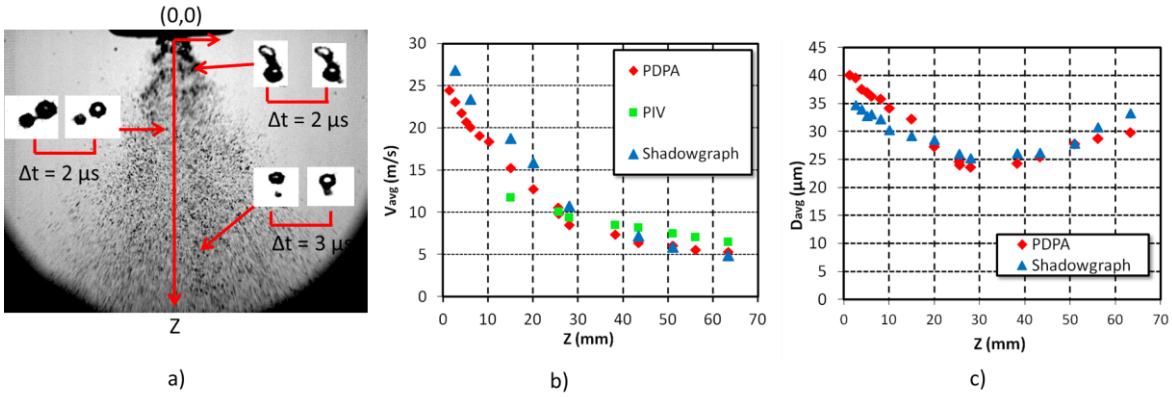

Figure 7: Instrument Comparison at Re_p = 15000 and $\dot{m}^*$ = 0.2 – a) Spray measurement zone, b) Velocity comparison, c) Diameter Comparison

Conclusion

The main objective of this study was to experimentally study the breakup characteristics of two pressure-swirl hydraulic as a function of Reynolds number. These two nozzles were classified as $\dot{m}^*$ = 0.2 and 0.29 with orifice diameter 0.3mm and 0.5mm, respectively. Liquid was injected into the testing zone at injection pressures ranging from 0.3-4MPa which correlated to a Reynolds number range of 7000-26000. This experimental study consisted of using three laser diagnostic techniques, Shadowgraph, PIV (Particle Image Velocimetry), and PDPA (Phase Doppler Particle Anemometry) to understand the breakup characteristic effects as a function of Reynolds number and non-dimensional mass flow rate and validation purposes. The findings are as followed:

- The cross-validation comparison between the three techniques compared well with each other, but limitations were found. It was observed that PDPA and Shadowgraph were only bounded by the film length and the first 1mm afterwards where ligament breakup took place. On the other hand, PIV was only appropriate in the later stages of secondary breakup and coalescence where the droplet density has been reduced.
- The film length was dependent on the maximum wave amplitude at breakup. The two nozzles experienced two different types of wave breakup. Both values had an asymptotic value that directly correlated to the spray cone angle as a constant.
- The average diameter decreased in a parabolic nature clearly illustrating the different breakup regimes. Reynolds number shifts the transition from one regime to another closer to the nozzles exit while also making the overall diameter smaller along the centerline. The change in $\dot{m}^*$ only shifted the curve downwards making the diameter smaller due to the higher momentum which allowed the droplets to become smaller to approach the critical Weber's number.
- The velocity had a constant decreasing slope for the first 25.4mm of the spray trajectory at which point the slopes decreased and became uniform towards the end. This was experienced for the increased Reynolds number and larger $\dot{m}^*$. The major difference occurred in the first 25.4mm zone where the slope was much higher for the larger Reynolds number and $\dot{m}^*$. While the zone after 25.4mm produced similar values for all Reynolds number and $\dot{m}^*$.

Acknowledgements

We would like to thank Parker Hannifin for providing UCF with their injector nozzles. This work was partially supported by US Air Force Research Laboratory.

References

[1] Cavaliere, A., Ragucci, R., Noviello, C., *Experimental Thermal and Fluid Science*, 27(4): 449-454(2003).
[2] Park, S.H., Kim, H.J.,Suh, H.K., Lee, C.S.,*Int. Journal Heat and Fluid Flow* 30: 960-970 (2009).
[3] Sivakumar, D., Kulkarni, V., *Journal of Experimental Fluids* 51: 587-596 (2011).
[4] El-Sayed, R.N., Hidaka, S., Kohno, M., Takata, Y,. *Int. Journal of Heat and Fluid Flow* 32: 95-106 (2011).
[5] Shi, H., Kleinstreuer, C., *Journal of Fluids Engineering* 129: 621-633 (2007).
[6] Faeth, G.M., Hsiang, L.P., Wu, P.K., *International journal of Multiphase Flow* 21: 99-127 (1995)
[7] Tratnig, A., Brenn, G.,Stirxner, T., Franhauser, P., Laubacher, N., Stranzinger, M., *Journal of Food Engineering* 95:126-134 (2009).
[8] Payri, R., Tormos, B., Salvado, F.J., Araneo, L., *Journal of Fuel* : 3176-3182 (2008).
[9] Kim, H.J., Suh, H.K., Park, S.H., Lee, C.S., *Energy & Fuels* 22: 2091-2098 (2008).
[10] Ahmed, M., Ashgriz, N., Tran, H.N., *Journal of Fluids Engineering* 131: (2009).
[11] Senecal, P.K., Schmidt, D.P., Nouar, I., Rutland, C.J., Reitz, R.D., *International Journal of Multiphase Flow* 25: 1073-1097 (1999).
[12] Kohnen, B.T., Musemic, E., Straßburger, F., Küpper, B., Walzel, P., *ILASS – Europe 2010, 23rd Annual Conference on Liquid Atomization and Spray Systems, Brno, Czech Republic*, September 2010.
[13] Wahono, S., Honnery, D., Soria, J., Ghojel, J., *Experiments in Fluids* 44: 451-459 (2008).
[14] Wierzba, A., *Experiments in Fluids* 9: 59-64 (1990).
[15] Sterling, A.M., and Sleicher, C.A., *Journal of Fluid Mechanics* 68: 477-495 (1975).
[16] Sedarsky, D., Paciaroni, M., Berrocal1, E., Petterson, P., Zelina, J.,Gord, J., and Linne, M., *Experiments in Fluids49: 391-408* (2010).